Chemical Engineering Science 270 (2023) 118551

Contents lists available at ScienceDirect

Chemical Engineering Science

journal homepage: www.elsevier.com/locate/ces

First-principles study of the effect of the local coordination environment on the electrochemical activity of Pd_1-C_xN_y single atom catalysts

Yun Huang [a], Chuwei Zhu [a], Jielou Liao [a], Xiang-Kui Gu [b,*], Wei-Xue Li [a,*]

[a] School of Chemistry and Materials Science, Hefei National Research Center for Physical Sciences at the Microscale, University of Science and Technology of China, Hefei, Anhui 230026, China
[b] School of Power and Mechanical Engineering, Wuhan University, Wuhan 430072, China

HIGHLIGHTS

- Effect of the local coordination environment on the HER and ORR activities of Pd_1-N_xC_y was studied by DFT calculations.
- Stability in terms of Pd formation energy was highly dependent on the local coordination environment.
- Changing the local coordination number and coordinated components can significantly impact the adsorption energies of intermediates.
- Promising HER and ORR electrocatalysts were designed through varying the local coordination environment.

GRAPHICAL ABSTRACT

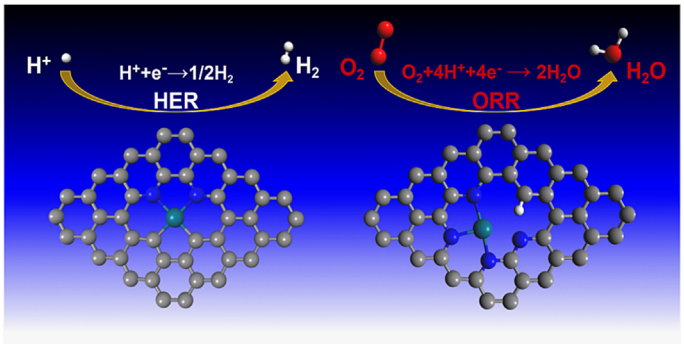

ARTICLE INFO

Article history:
Received 1 January 2023
Received in revised form 2 February 2023
Accepted 6 February 2023
Available online 10 February 2023

Keywords:
Single atom catalyst
Coordination number
Coordinated component
Electrochemical activity
DFT calculations

ABSTRACT

Development of more efficient HER and ORR electrocatalysts is crucial for the production and utilization of H_2 as a clean and sustainable energy carrier. M–N–Cs based single-metal-atom electrocatalysts have been extensively reported to be the alternatives to cost-ineffective Pt electrocatalysts, and their activities were significantly sensitive to the local coordination environment, but the underlying mechanism is still unclear yet. Herein, effects of the local coordination numbers and coordinated components of a single Pd atom in Pd_1-N_xC_y on the HER and ORR activities were systematically investigated using theoretical calculations. We found that change in the local coordination environment is an effective way to modulate the electrochemical activities, and the four-atom-coordinated Pd_1-N_2C_2-2 and the three-atom-coordinated Pd_1-N_3C_0-3 were the most promising HER and ORR electrocatalysts, respectively. This work provides valuable insights into designing more efficient M–N–Cs electrocatalysts for HER and ORR, as well as the other important electrochemical processes.

© 2023 Elsevier Ltd. All rights reserved.

1. Introduction

The development of clean and sustainable technologies to produce fuels and chemicals of global importance has attracted extensive attention due to the rapid depletion of fossil fuels and the large emissions of pollutants during the utilization of the traditional energy resources (Chu et al., 2017; Dusastre, 2010; Millet et al., 2010; Steele and Heinzel, 2001). As a clean energy molecule, H_2 can be produced from the electrochemical water splitting process via the cathodic hydrogen evolution reaction (HER) using the electric energy (Nørskov et al., 2005; Lasia, 2010; Zheng et al., 2015) that is generated from the clean and renewable

* Corresponding authors.
E-mail addresses: xiangkuigu@whu.edu.cn (X.-K. Gu), wxli70@ustc.edu.cn (W.-X. Li).

https://doi.org/10.1016/j.ces.2023.118551
0009-2509/© 2023 Elsevier Ltd. All rights reserved.

resources (i.e., solar and wind). The chemical energy that is stored in the H−H bond of the produced H_2 can then be converted to the electric energy using the pollution-free fuel cell technologies, in which the sluggish cathodic oxygen reduction reaction (ORR) generally determines their overall performance (Debe, 2012; Perry and Fuller, 2002). In the electrochemical circulation of H_2 production and utilization, the cathodic electrocatalysts of the related electrochemical devices play important roles in the improvement and popularization of the advocated hydrogen economy. Thus, the exploration of more efficient electrocatalysts for HER and ORR has been widely investigated (Jiao et al., 2015; Mahmood et al., 2017; Seh et al., 2017; Vij et al., 2017; Yuan et al., 2020) to overcome the cost-ineffective nature of the traditionally utilized the state-of-the-art Pt/C catalyst (Lefèvre et al., 2009; Wu et al., 2011).

Single atom catalysts (SACs) have attracted significant research interest for a wide range of electrocatalytic reactions including HER and ORR, due to their intriguing properties, such as high metal atom utilization efficiency, controlled coordination environments of metal atoms, unique quantum size effects, and tunable metal − support interactions (Chen et al., 2018a; Fei et al., 2019; Zhang et al., 2019). In particular, graphene-based electrocatalysts commonly exhibit an enhanced electrochemical performance owing to their distinctive structural merits, including a large surface area, high electrical conductivity, and good chemical stability (Fei et al., 2019; Huang et al., 2019). Amongst, the M−N−C−base electrocatalysts, where M, N, and C respectively refer to the metal, nitrogen, and carbon atoms, have shown excellent catalytic activities for ORR and HER. For instance, Wang et al. fabricated Fe−N−C SACs that exhibited a high oxygen reduction performance with the same activity as Pt/C electrocatalyst in the fuel cells and zinc–air batteries (Chen et al., 2018b). Chen and co-workers developed a facile zeolitic imidazolate framework (ZIF)-driven strategy for Co−N−C SACs that outperformed benchmark Pt catalyst for pH-universal HER (Chen et al., 2021a). In addition, M−N−Cs are also promising catalysts for other important electrochemical processes, such as CO_2/CO reduction (Tripkovic et al., 2013) and N_2 reduction (Li et al., 2016). Although lots of efforts have been made to elucidate the roles of different single metal atoms in affecting the catalytic activity of M−N−Cs, the influence of the local coordination environment of the single metal atom on the electrochemical activity is still not well understood yet (Wang et al., 2021). Generally, the single metal atom was not the sole active site for the intermediates adsorption, and it required to cooperate with the coordinated other components to catalyze the reactions (Vilé et al., 2015; Wang et al., 2017). These local coordination environments including the coordination number and the coordinated components also played a vital role in governing the catalytic activity (Fei et al., 2018; Ha et al., 2021; Li et al., 2019b; Wang et al., 2020b). However, the underlying mechanism of the local coordination environmental effect on the activity of M−N−Cs is still unclear, limiting the design of more efficient electrocatalysts.

To realize the rational design of the novel electrocatalysts for the cathodic HER and ORR, herein, the influence of the local coordination environment of Pd_1-N_xC_y on the HER and ORR activities was systematically studied by means of density functional theory (DFT) calculations. The coordination numbers of 3 and 4 for Pd was considered with varied coordination components (different numbers of N and C atoms). The formation energies of a single Pd atom in distinct coordination environments were calculated to evaluate the stability of Pd, and the adsorption free energies of the HER and ORR intermediates, as well as their theoretical overpotentials were determined to understand the dependence of the catalytic activities on the local coordination environment. We found that the change in the local coordination number and coordination component of Pd can highly impact on the adsorption site and adsorption strengths of the intermediates, consequently affecting the HER and ORR activity, and providing an effective way in designing more efficient electrocatalysts, such Pd_1-N_2C_2-2 on Pd_1-N_3C_0-3 for HER and ORR, respectively.

2. Computational methods

Periodic DFT calculations were performed using the Vienna Ab initio Simulation Package (Kresse and Furthmüller, 1996), at the level of generalized gradient approximation (GGA) using optB86b van der Waals (vdW) exchange–correlation functional (Klimeš et al., 2011). The Kohn-Sham valence states were expanded in a plane wave basis set with a kinetic energy cutoff of 400 eV. The graphene was modeled using slab of a free-standing graphene with a (5×5) supercell, containing a total of 50C atoms. A vacuum space of $\sim$ 20 Å in the z direction was set to avoid the artificial interactions between the repeated slabs. Brillouin zone was sampled with a Γ-centered ($3 \times 3 \times 1$) k-point mesh (Monkhorst and Pack, 1976). To model the less defective surfaces, a carbon vacancy dimer (a pair of adjacent C vacancies) was created to stabilize Pd atom, which is coordinated with a total number of 4 adjacent C or N atoms (C/N ratio varies from 0 to 4). To model the more defective surfaces, one more adjacent C vacancy was created on the carbon vacancy dimer surface, Pd atom is coordinated with a total number of 3 adjacent C or N atoms. During the optimization, all the atoms were allowed to be relaxed until the force was less than 0.02 eV/Å.

To evaluate the stability of the single Pd atom against its aggregation, the formation energy was calculated as (Gao et al., 2020)

$$E_f = E(Pd_1\text{-}N_xC_y) - E(N_xC_y) - E(Pd) \quad (1)$$

where E(Pd) is the energy of Pd atom in bulk Pd, $E(Pd_1\text{-}N_xC_y)$ is the energy of the optimized Pd_1-N_xC_y structure, and $E(N_xC_y)$ is the energy of *N*-doped graphene.

For the cathodic HER and ORR, the adsorption free energies of the reaction intermediates were calculated as

$$\Delta G_{H^*} = G(H^*) - G(^*) - 1/2G_{H2} \quad (2)$$

$$\Delta G_{O^*} = G(O^*) - G(^*) - (G_{H2O} - G_{H2}) \quad (3)$$

$$\Delta G_{OH^*} = G(OH^*) - G(^*) - (G_{H2O} - 1/2G_{H2}) \quad (4)$$

$$\Delta G_{OOH^*} = G(OOH^*) - G(^*) - (2G_{H2O} - 3/2G_{H2}) \quad (5)$$

7where G(H*), G(O*), G(OH*), and G(OOH*) refer to the free energy of the adsorbed H*, O*, OH*, and OOH*, respectively, and the zero-point energy correction and the entropic contribution were considered. For HER, the theoretical overpotential η was calculated as (Xu et al., 2018)

$$\eta^{HER} = |\Delta G_{H^*}|/e \quad (6)$$

For ORR, the reaction free energy (ΔG_1, ΔG_2, ΔG_3, ΔG_4) for each step as shown in Supplementary Material (reaction S2-S5) was calculated as(Chen et al., 2021b; Ha et al., 2021)

$$\Delta G_1 = \Delta G_{OOH^*} - 4.92 \quad (7)$$

$$\Delta G_2 = \Delta G_{O^*} - \Delta G_{OOH^*} \quad (8)$$

$$\Delta G_3 = \Delta G_{OH^*} - \Delta G_{O^*} \quad (9)$$

$$\Delta G_4 = -\Delta G_{OH^*} \quad (10)$$

The theoretical overpotential was determined as (Chen et al., 2021b; Ha et al., 2021)

$$\eta^{ORR} = 1.23 + [\max(\Delta G_1, \Delta G_2, \Delta G_3, \Delta G_4)]/e \quad (11)$$

3. Results and discussion

3.1. Effect of the local coordination environment on the stability of Pd_1-N_xC_y

The formation of stable single Pd atom in the *N*-doped graphene is a prerequisite for its further utilization as an electrocatalyst in the HER and ORR processes, and thus the influence of the local coordination environment of Pd involving the coordination number and the coordinated components on the structural stability was systematically investigated first. For the N atom doping in the graphene, it generally can form the pyridinic, pyrrolic, and graphitic structures, and the pyridinic N structure was used to stabilize the Pd atom here, owing to it has been widely reported to be more active for the electrochemical reactions (Bi et al., 2016; Li et al., 2019a; Liu et al., 2020; Nie et al., 2016; Wang et al., 2020a). Additionally, the coordination numbers of Pd being 3 and 4 were focused, since they were the typical coordination numbers for the experimentally synthesized M−N−Cs (Fei et al., 2018; Sultan et al., 2019; Tiwari et al., 2018; Xu et al., 2022). Based on these and with the considerations of the different numbers of N atoms ($0 \sim 4$) as well as their relative positions in the doped systems, a total number of 35 Pd_1-N_xC_y were constructed.

To evaluate the stability of these constructed single Pd atoms, their formation energies were calculated, and the more negative energy value means that the structure is more stable. For the four-atom-coordinated Pd (Fig. 1), the calculated formation energies were $-1.83 \sim -3.04$ eV (Table S1), suggesting that these structures were thermodynamically very stable (Gao et al., 2020), and Pd_1-N_2C_2-2 exhibited the most stable nature with the most negative formation energy among these, similar results have also been reported (Ha et al., 2021). We note that when Pd only coordinated with C atoms in Pd_1-N_0C_4, a non-planar structure with Pd atom being pulled out the graphene surface could be formed, resulting in a less stable structure with a formation energy of −0.59 eV.

For the three-atom-coordinated Pd (Figs. S1-3), three types structures were constructed, including Pd_1-N_1C_2-n, Pd_1-N_2C_1-n, and Pd_1-N_3C_0-n. When we fixed the positions of the N atoms that coordinated with Pd and varied the positions of the other N atoms, three groups (n = $1 \sim 4$, n = $5 \sim 8$, and n = $9 \sim 12$) can be classified among these structures. In every group, it was found that the calculated formation energy became gradually more negative as the averaged bond length became shorter (Fig. 2a), resulting in the most stable structures with the n values being 4, 8 and 12 (Tables S2-4), which possessed the highest N doping content in each group. In addition, Fig. 2b clearly showed that the Bader charge of Pd became gradually positive as the formation energy became more negative. These demonstrated that the local environment of single Pd atom in the *N*-doped graphene not only highly affected the stability of Pd but also its electronic structure, and consequently its catalytic property.

3.2. Effect of the local coordination environment on HER activity

To understand the effect of the local environment of single Pd atoms on their electrochemical activity, HER was studied on these constructed structures. For H atom adsorption on these structures, various adsorption sites have been considered, and it was found that the H atom prefers to bind to the C atoms that coordinated with Pd on the four-atom-coordinated Pd_1-N_xC_y (Fig. 3), and three-atom-coordinated Pd_1-N_1C_2-n and Pd_1-N_2C_1-n (Figs. S4 and S5), suggesting that the single Pd atom was not the active site for HER, however, the single Pd atom can play a indirect role in affecting the HER activity through affecting the electronic structures of the coordinated C atoms. On the Pd_1-N_3C_0-n systems, the single Pd atom in turn can directly tune the activity of HER, owing to that the H atom tends to bind to the single Pd atom (Fig. S6). For the H atom adsorption on the four-atom-coordinated Pd_1-N_xC_y, we found that it was an exothermic process on Pd_1-N_1C_3 and Pd_1-N_2C_2-3 with Pd_1-N_1C_3 exhibiting the strongest adsorption free energy of

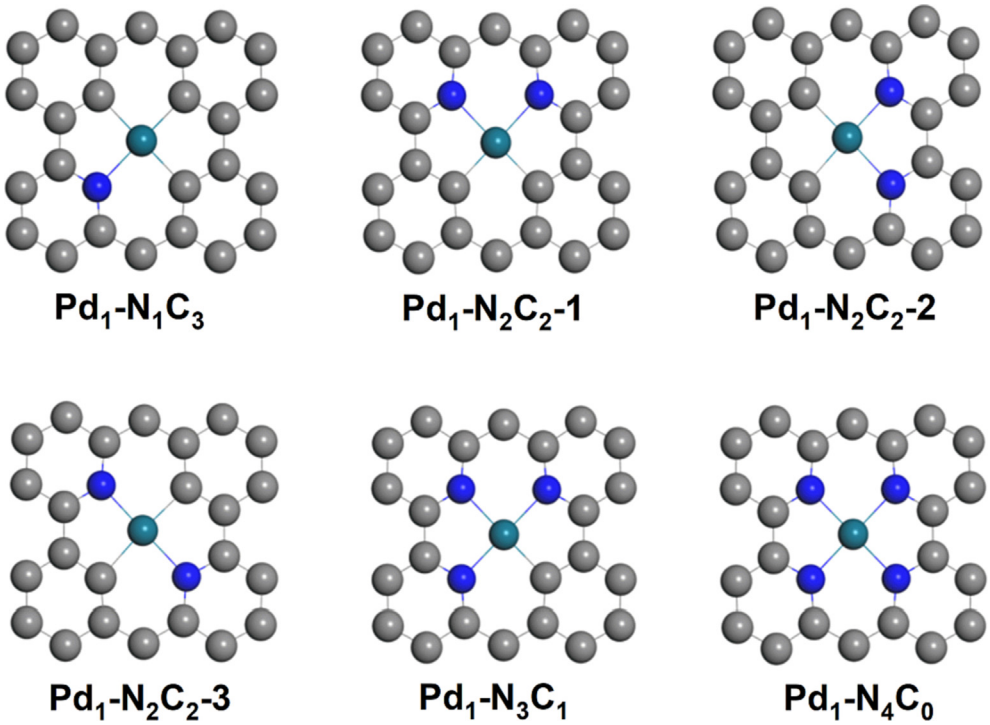

Fig. 1. Optimized geometric structures of four-coordinated Pd_1-N_xC_y. The gray, blue, cyan spheres represent C, N, and Pd atoms, respectively.

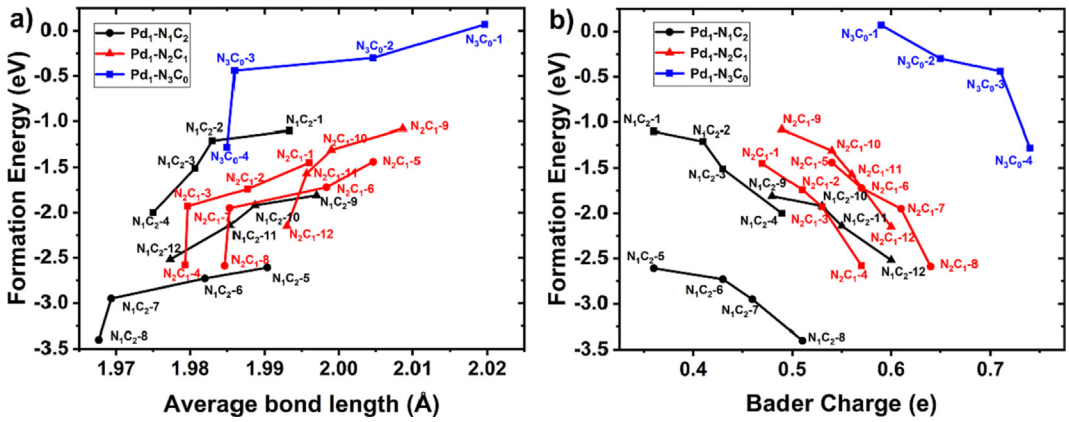

Fig. 2. Correlations between the formation energy and the averaged Pd-N/C bond length (a) and the Bader charge of Pd (b) in the three-atom-coordinated Pd_1-N_xC_y.

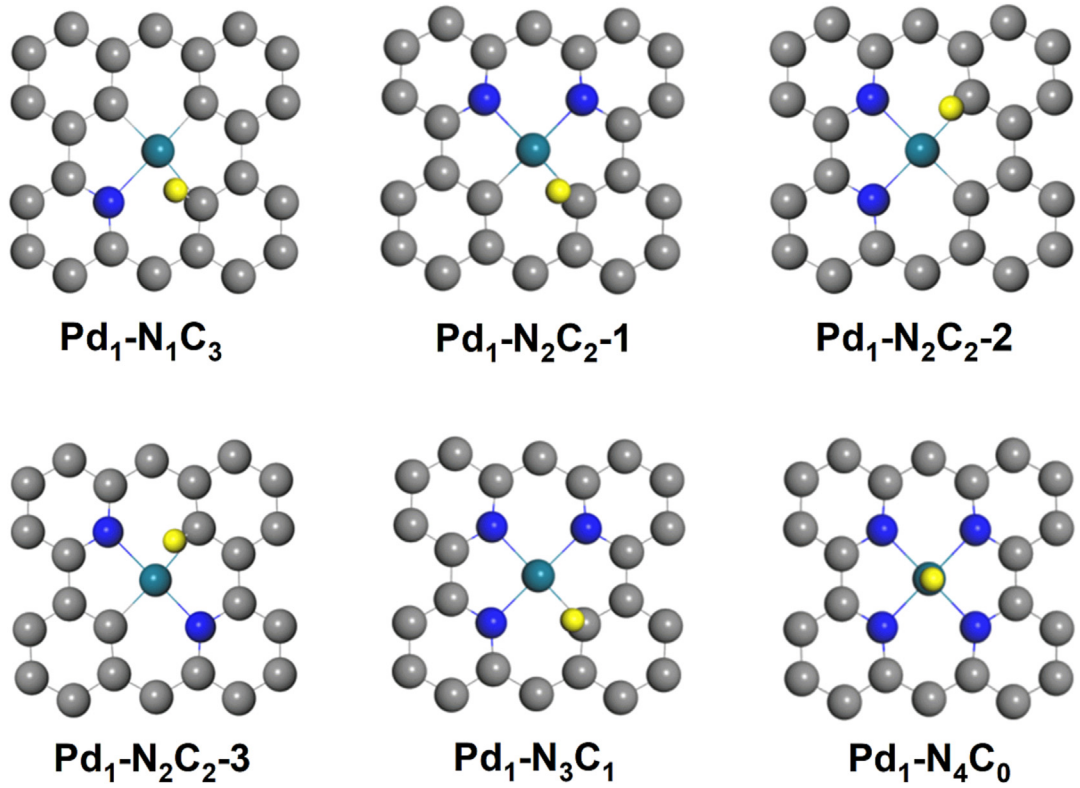

Fig. 3. Optimized most stable geometric structures of H adsorption on the four-atom-coordinated Pd_1-N_xC_y. The gray, blue, cyan, and yellow spheres represent C, N, Pd, and adsorbed H atoms, respectively.

−0.94 eV (Table S5 and Fig. 4). While on the other systems, it was an endothermic process, and Pd_1-N_4C_0 exhibited the weakest adsorption free energy of 1.77 eV, implying that this structure is not active for HER with much higher theoretical overpotential. Interestingly, it was found that although the H atom adsorption on Pd_1-N_2C_2-2 was also slightly endothermic, the adsorption free energy (0.02 eV) very close to the optimal energy (0 eV) for HER, giving rise to this structure could be a very promising HER electrocatalyst (Fig. 4b).

In the case of the H atom adsorption on Pd_1-N_1C_2-n systems, it was found that this process on Pd_1-N_1C_2-5 (0.44 eV) and Pd_1-N_1C_2-6 (0.36 eV) was endothermic, while it was exothermic on the remained systems (Table S6). The strongest adsorption was found to be at Pd_1-N_1C_2-10 with an adsorption free energy of −0.84 eV, resulting in a highest theoretical overpotential and lowest HER activity among these systems (Fig. 4). On Pd_1-N_1C_2-7 and Pd_1-N_1C_2-8, the adsorption free energies of the H atom were slightly exothermic by 0.03 and 0.08 eV, respectively, suggesting that these two systems were the most promising HER electrocatalysts for Pd_1-N_1C_2-n. For Pd_1-N_2C_1-n systems, we found that only Pd_1-N_2C_1-9 and Pd_1-N_2C_1-10 exhibited negative adsorption free energies of H (Table S7), while the other systems were difficult for an effective H adsorption with positive adsorption free energies, especially for Pd_1-N_2C_1-n (n = 1 ∼ 8), the free energies were too weak for HER. Similarly, the H atom adsorption on Pd_1-N_3C_0-n systems was also very weak with the calculated adsorption free energies being more than 0.72 eV (Table S8), implying that the positively charged single Pd atom was not active for HER.

Fig. 4 showed the free energy diagrams and the calculated theoretical overpotentials for HER on the considered Pd_1-N_xC_y electro-

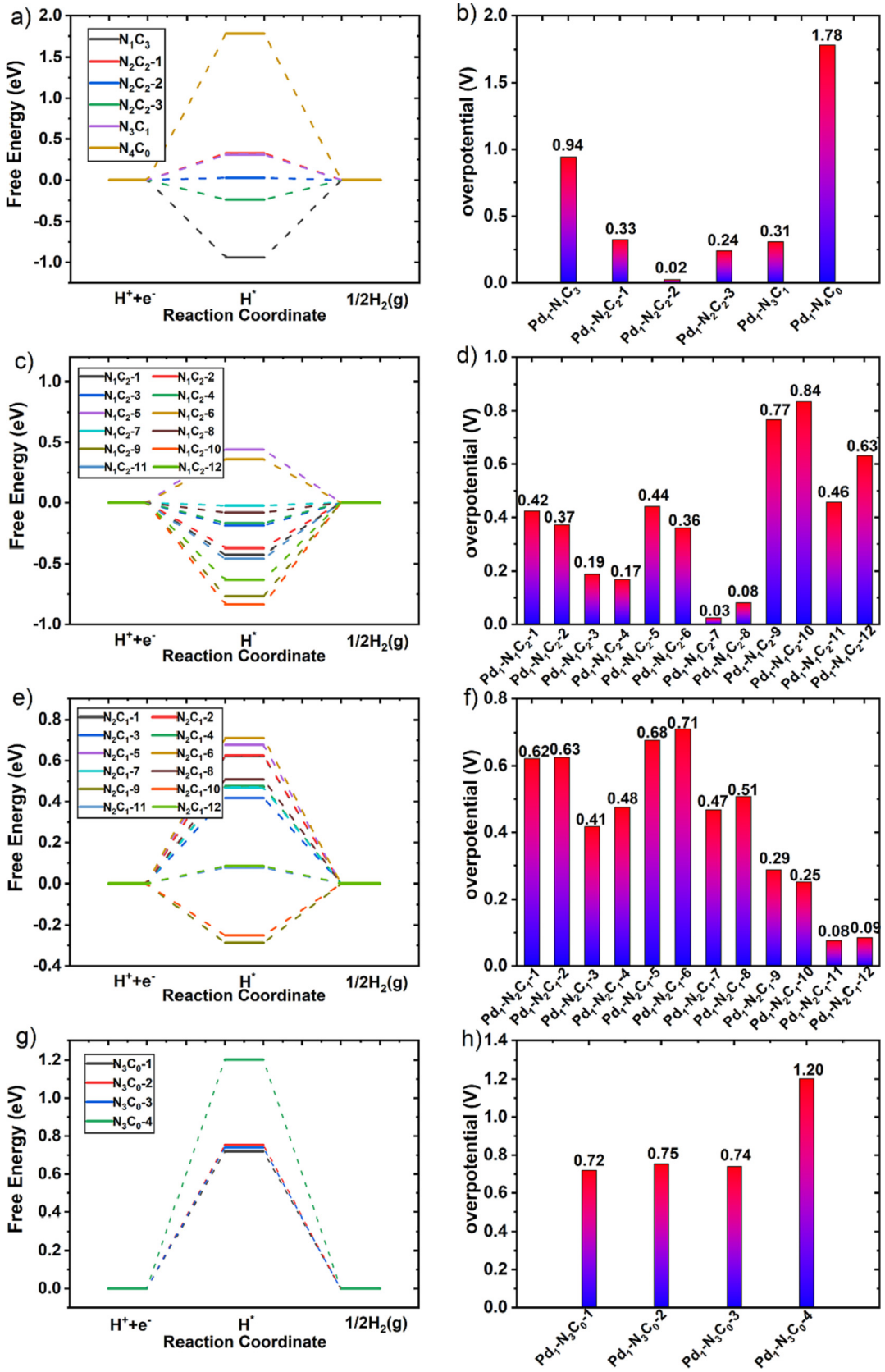

Fig. 4. Free energy diagrams and the calculated theoretical overpotentials for HER on Pd_1-N_xC_y.

catalysts, where we can easily find that the HER activity was highly dependent on the local coordination environment of the single Pd atom, owing to this would result in a very distinct electronic structure of Pd that can further highly impact the catalytic activity of the coordinated C atoms, which were the active sites for HER on the majority of the studied systems. Among all these systems, it

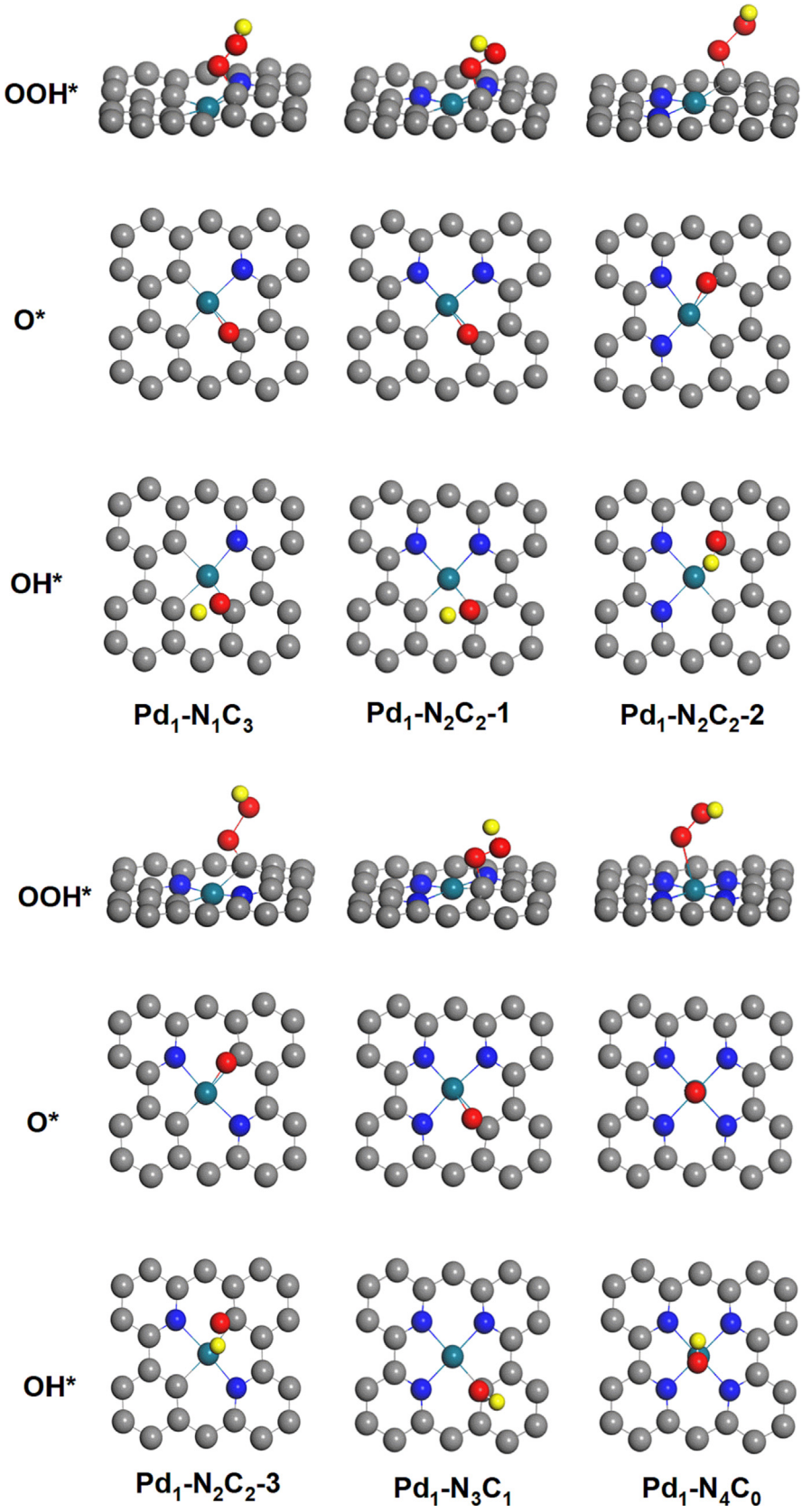

Fig. 5. Optimized most stable geometric structures of OOH, O, and OH adsorption on the four-atom-coordinated Pd_1-N_xC_y. The gray, blue, cyan, red and yellow spheres represent C, N, Pd, O, and H atoms, respectively.

was found that four-atom-coordinated Pd_1-N_2C_2-2, and three-atom coordinated Pd_1-N_1C_2-7, Pd_1-N_1C_2-8, Pd_1-N_2C_1-11, and Pd_1-N_2C_1-12 were the promising HER electrocatalysts, exhibiting an overpotential of less 0.10 V, given that the traditionally used Pt catalyst exhibited a calculated overpotential of 0.22 V on Pt(1 1 1).

3.3. Effect of the local coordination environment on ORR activity

The local coordination environment influence on the activity of the cathodic ORR in the H_2 fueled fuel cell mode was also investigated. For the adsorption of the OOH*, O*, and OH* intermediates involved in ORR, on the four-atom-coordinated Pd_1-N_xC_y (except for Pd_1-N_4C_0), we found that OOH* and OH* tend to bind to the top site of the C atom that coordinated with the Pd atom, while the O* atom prefers to bind to the bridge site between Pd and C (Fig. 5). On Pd_1-N_4C_0, the top site of Pd was found to be the most stable site for the adsorption of these species. Amongst, Pd_1-N_4C_0 exhibited the weakest adsorption free energies, and Pd_1-N_1C_3 exhibited the strongest ones (Table S5). For ORR at a typical condition of 0.8 V vs RHE, it was found that the OOH* formation ($* + O_2(g) + H^+ + e^- \rightarrow OOH^*$) was the most endothermic reaction on Pd_1-N_4C_0, suggesting that this step is the potential determining step, owing to the weaker adsorption nature of this system. However, the potential determining step turns to be the OH* formation ($O^* + H^+ + e^- \rightarrow OH^*$) on the other systems, resulting in the weaker adsorption of O* would give a higher ORR activity, such as that on Pd_1-N_3C_1. On these systems, we found that Pd_1-N_3C_1 exhibited the lowest theoretical overpotential of 0.73 V, and the overpotentials on the remained systems were too high to be active for ORR.

On the three-atom-coordinated Pd_1-N_1C_2-n, the Pd-C bridge site was also found to be most favorable for O* adsorption (Fig. S7), and Pd_1-N_1C_2-10 and Pd_1-N_1C_2-3 showed the strongest and weakest adsorption free energies (Table S6), respectively. However, the most favorable adsorption sites for OOH* and OH* were dependent on the local structures of these systems. The OOH* species tends to adsorb at the top site of Pd on Pd_1-N_1C_2-10, while it prefers to adsorb at the top site of C coordinated with Pd on the remained systems. For OH* adsorption, the Pd top sites of Pd_1-N_1C_2-5 and Pd_1-N_1C_2-6, and the Pd-C bridge site of Pd_1-N_1C_2-10 were the most stable sites, while the top site of C coordinated with Pd was the most stable one on the other systems. Based on the calculated theoretical overpotential (Fig. 6b), we can find that Pd_1-N_1C_2-n (n = 1 ~ 4) exhibited higher ORR activity (lower overpotential) than the other systems, especially for Pd_1-N_1C_2-3, which gave a lowest overpotential of 0.54 V amongst, demonstrating that it would be a potential candidate for efficient ORR.

For OOH* adsorption on Pd_1-N_2C_1-n (Fig. S8), the most stable site was the top site of Pd on Pd_1-N_2C_1-6、Pd_1-N_2C_1-7 and Pd_1-N_2C_1-8, and it tends to adsorb at the top site of C coordinated with Pd on the remained systems. The top site of C and the Pd-C bridge site were both found to be facile for stabilizing the O* intermediate, and the bridge site was the most stable on Pd_1-N_2C_1-n (n = 4 ~ 8). We note that the Pd-C bond was broken when O* adsorbed on Pd_1-N_2C_1-n (n = 5 ~ 8) with an O* inserting between them, resulting in a less stable structure. The most stable site for OH* adsorption was the top site of the C atom coordinated with Pd on all these systems. The calculated theoretical overpotential showed that Pd_1-N_2C_1-n (n = 5 ~ 8) exhibited the higher overpotential and lower ORR activity, and Pd_1-N_2C_1-11 possessed the highest ORR activity (Fig. 6c). On Pd_1-N_3C_0-n, all these intermediates tend to adsorb at the top site of the single Pd atom (Fig. S9), suggesting that the electronic property of Pd would be a dominant factor in governing the ORR activity. The OOH* formation ($* + O_2(g) + H^+ + e^- \rightarrow OOH^*$) was determined to be the potential determining step for ORR on Pd_1-

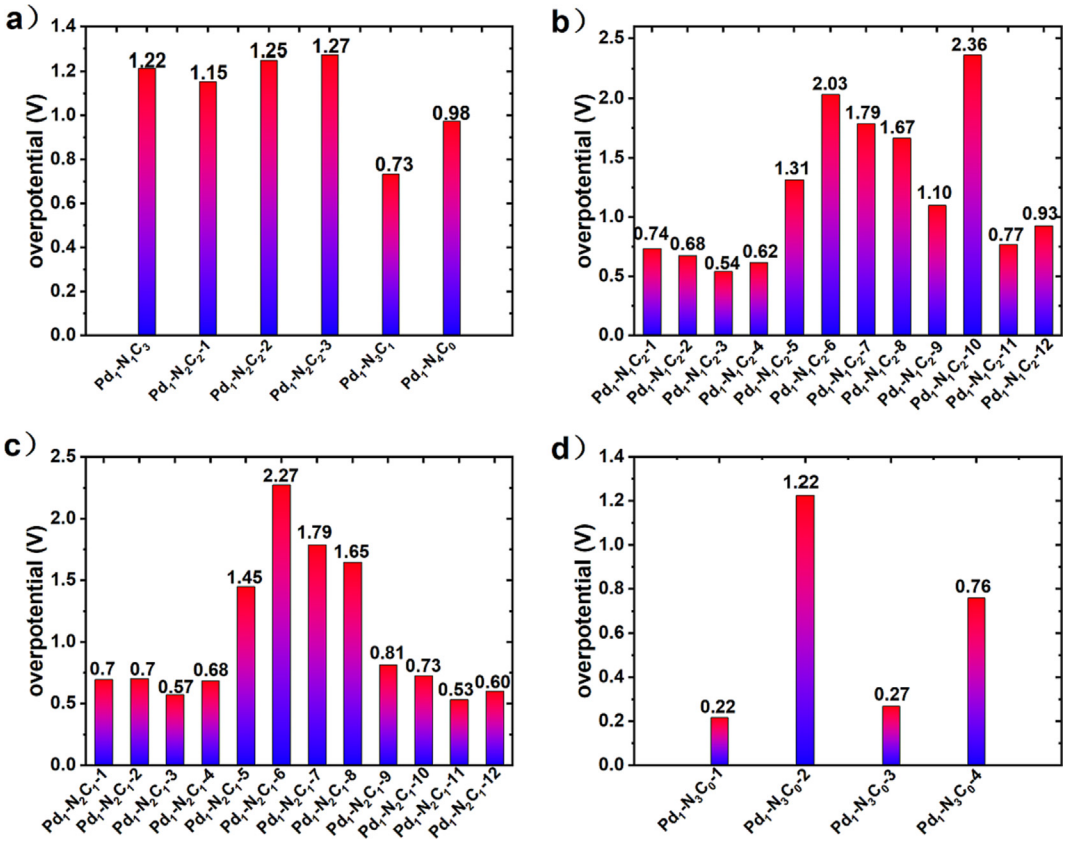

Fig. 6. Calculated theoretical overpotential for ORR on Pd_1-N_xC_y.

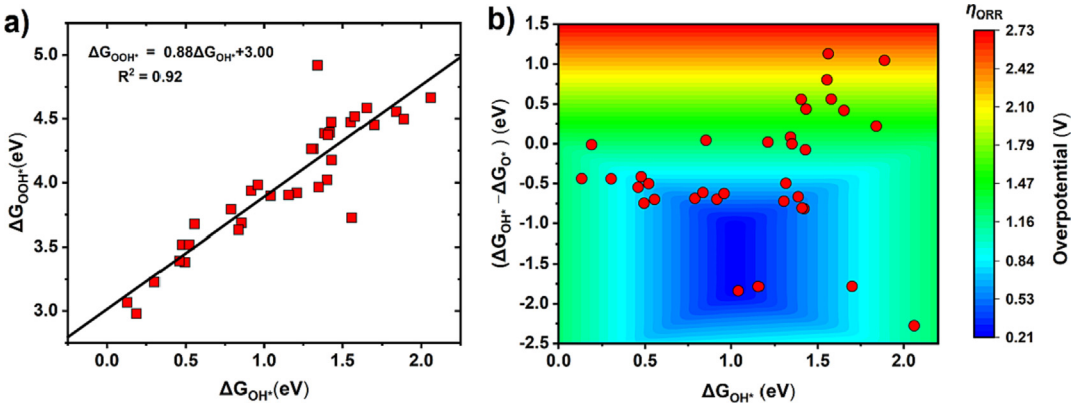

Fig. 7. (a) Linear correlation between the adsorption free energies of OOH* and OH*. (b) Colored counter plot of ORR activity showing the relationship between ORR theoretical overpotential and ΔG_{OH^*} and ($\Delta G_{OH^*} - \Delta G_{O^*}$) on Pd_1-N_xC_y.

N_3C_0-n, the stronger adsorption of this species on Pd_1-N_3C_0-1 and Pd_1-N_3C_0-3 resulted in a lower overpotential. In fact, the calculated respective overpotentials of 0.22 and 0.27 V on Pd_1-N_3C_0-1 and Pd_1-N_3C_0-3 were significantly lower than that on the other Pd_1-N_xC_y considered. The much lower overpotential suggested that these two electrocatalysts were very promising for ORR. Taking into account of the structural stability, the formation energy of the single Pd atom in Pd_1-N_3C_0-1 was slightly positive (not structurally stable), Pd_1-N_3C_0-3 would be more appropriate as the ORR electrocatalysts.

To better understand the relationship between the ORR activity and the adsorption free energies of the intermediates, the correlation between the adsorption free energies of OOH* and OH* was studied, which were considered as the key intermediates to determine the ORR activity. Actually, it was previously reported that the linear relationship of $\Delta G_{OOH^*} = \Delta G_{OH^*} + 3.2 \pm 0.2$ eV was found to be universal for OOH* and OH* adsorbed on the surfaces of metals and their metallic alloys (Seh et al., 2017). While the universality of this relationship on the single atoms with various local coordination environments is still unclear. Thus, ΔG_{OOH^*} against ΔG_{OH^*} on all the considered Pd_1-N_xC_y was analyzed, and a similar good linear relationship of $\Delta G_{OOH^*} = 0.88\Delta G_{OH^*}+3.00$ was obtained (Fig. 7a), consistent with that on TM−BH (Singh et al., 2018) and TM−N−C (Xu et al., 2018) systems with various TM atoms. This suggested that the local coordination environment of single atom has limited effect on the correlation of the intermediates adsorption free energies, though it exhibited significant influence on the individual adsorption free energy.

Invoking the linear expression between ΔG_{OOH^*} and ΔG_{OH^*}, Equations (7) to (10) can be rewritten as

$$\Delta G_1 = (0.88\Delta G_{OH*}+3.00) - 4.92 \quad (11)$$

$$= 0.88\Delta G_{OH*} - 1.92 \quad (12)$$

$$\Delta G_2 = \Delta G_{O*} - (0.88\Delta G_{OH*}+3.00) \quad (13)$$

$$= -(\Delta G_{OH*} - \Delta G_{O*}) + 0.12\Delta G_{OH*} - 3.00 \quad (14)$$

$$\Delta G_3 = \Delta G_{OH*} - \Delta G_{O*} \quad (15)$$

$$\Delta G_4 = -\Delta G_{OH*} \quad (16)$$

It is obvious that ΔG_1, ΔG_2, ΔG_3 and ΔG_4 were determined by two variables, ΔG_{OH^*} and ($\Delta G_{OH^*} - \Delta G_{O^*}$).Therefore, these two variables can be used as the descriptors to predict η^{ORR} (Chen et al., 2021b; Singh et al., 2018). The volcano plot shown in Fig. 7b clearly exhibited a function between η^{ORR} and two descriptors of ΔG_{OH^*} and ($\Delta G_{OH^*} - \Delta G_{O^*}$). The dark blue part of the plot showed the region of the highest ORR activity with a η^{ORR} of 0.21 V under the optimum condition of $\Delta G_1 = \Delta G_4 = -1.02$ eV, suggesting that the catalyst that sites this point should theoretically exhibit the highest ORR activity among this kind of catalyst. For the considered Pd_1-N_xC_y, Pd_1-N_3C_0-3 was found to be closer this point with a η^{ORR} of 0.27 V, smaller than that of the calculated 0.57 V on Pt(111), implying that this catalyst might be more active for ORR than the state-of-the-art Pt catalyst.

4. Conclusions

Effect of the local coordination environment of the single Pd atom embedded in the *N*-doped graphene on the electrochemical activity of HER and ORR was systematically studied by DFT calculations, via varying the coordination numbers and coordination components of Pd. We found that although the local coordination environment can highly affect the formation energy of the single Pd atom, almost all the structures considered were thermodynamically stable, suggesting that changing the local coordination environment was an effective way to create the novel stable structures of Pd_1-N_xC_y. For HER, we found that the single Pd atom played an indirect role in affecting the HER activity, through tuning the catalytic property of the coordinated C atom, which was active for the H atom adsorption on the promising Pd_1-N_xC_y. While the single Pd atom can directly impact the ORR activity, owing to it can act as the active site for the intermediates adsorption. Among the structures studied, we found that Pd_1-N_2C_2-2 and Pd_1-N_3C_0-3 were the most promising electrocatalysts for HER and ORR, respectively, with significantly lower overpotentials. This work provides valuable insight into the designing more efficient M−N−C electrocatalysts for the cathodic HER and ORR, as well as the other related electrochemical reactions.

CRediT authorship contribution statement

Yun Huang: Investigation, Writing – original draft, Data curation. **Chuwei Zhu:** Formal analysis. **Jielou Liao:** Formal analysis. **Xiang-Kui Gu:** Conceptualization, Supervision, Writing – review & editing. **Wei-Xue Li:** Conceptualization, Supervision, Writing – review & editing.

Data availability

The data that has been used is confidential.

Declaration of Competing Interest

The authors declare that they have no known competing financial interests or personal relationships that could have appeared to influence the work reported in this paper.

Acknowledgments

This work was supported by the National Key R&D Program of China (2018YFA0208603), the National Natural Science Foundation of China (22221003, 22273068), K. C. Wong Education (GJTD-2020-15). The authors also gratefully thank Supercomputing Center of University of Science and Technology of China and Wuhan University.

Appendix A. Supplementary material

Supplementary data to this article can be found online at https://doi.org/10.1016/j.ces.2023.118551.

References

Bi, Q.Y., Lin, J.D., Liu, Y.M., He, H.Y., Huang, F.Q., Cao, Y., 2016. Dehydrogenation of formic acid at room temperature: boosting palladium nanoparticle efficiency by coupling with pyridinic-nitrogen-doped carbon. Angew. Chem. Int. Ed. 55 (39), 11849–11853.
Chen, Y., Ji, S., Chen, C., Peng, Q., Wang, D., Li, Y., 2018a. Single-atom catalysts: synthetic strategies and electrochemical applications. Joule 2 (7), 1242–1264.
Chen, Y., Ji, S., Zhao, S., Chen, W., Dong, J., Cheong, W.C., Li, Y., 2018b. Enhanced oxygen reduction with single-atomic-site iron catalysts or a zinc-air battery and hydrogen-air fuel cell. Nat. Commun. 9 (1), 1–12.
Chen, Z., Qing, H., Wang, R., Wu, R., 2021a. Charge pumping enabling Co–NC to outperform benchmark Pt catalyst for pH-universal hydrogen evolution reaction. Energ. Environ. Sci. 14 (5), 3160–3173.
Chen, X., Zhang, Y., Hu, R., Qing, S., Zhang, H., 2021b. DFT study of C2N-supported Ag3M (M= Cu, Pd, and Pt) clusters as potential oxygen reduction reaction catalysts. Chem. Eng. Sci. 239, 116642.
Chu, S., Cui, Y., Liu, N., 2017. The path towards sustainable energy. Nat. Mater. 16 (1), 16–22.
Debe, M.K., 2012. Electrocatalyst approaches and challenges for automotive fuel cells. Nature 486 (7401), 43–51.
Dusastre, V. (Ed.), 2010. Materials for Sustainable Energy: a Collection of Peer-Reviewed Research and Review Articles From Nature Publishing Group. World Scientific.
Fei, H., Dong, J., Feng, Y., Allen, C.S., Wan, C., Volosskiy, B., Huang, Y., 2018. General synthesis and definitive structural identification of MN4C4 single-atom catalysts with tunable electrocatalytic activities. Nat. Catal. 1 (1), 63–72.
Fei, H., Dong, J., Chen, D., Hu, T., Duan, X., Shakir, I., Duan, X., 2019. Single atom electrocatalysts supported on graphene or graphene-like carbons. Chem. Soc. Rev. 48 (20), 5207–5241.
Gao, J., bin Yang, H., Huang, X., Hung, S. F., Cai, W., Jia, C., & Liu, B., 2020. Enabling direct H2O2 production in acidic media through rational design of transition metal single atom catalyst. Chem 6 (3), 658–674.
Ha, M., Kim, D.Y., Umer, M., Gladkikh, V., Myung, C.W., Kim, K.S., 2021. Tuning metal single atoms embedded in N_xC_y moieties toward high-performance electrocatalysis. Energ. Environ. Sci. 14 (6), 3455–3468.
Huang, H., Yan, M., Yang, C., He, H., Jiang, Q., Yang, L., Yamauchi, Y., 2019. Graphene nanoarchitectonics: recent advances in graphene-based electrocatalysts for hydrogen evolution reaction. Adv. Mater. 31 (48), 1903415.
Jiao, Y., Zheng, Y., Jaroniec, M., Qiao, S.Z., 2015. Design of electrocatalysts for oxygen-and hydrogen-involving energy conversion reactions. Chem. Soc. Rev. 44 (8), 2060–2086.
Klimeš, J., Bowler, D.R., Michaelides, A., 2011. Van der Waals density functionals applied to solids. Phys. Rev. B 83, (19) 195131.
Kresse, G., Furthmüller, J., 1996. Efficient iterative schemes for ab initio total-energy calculations using a plane-wave basis set. Phys. Rev. B 54 (16), 11169.
Lasia, A., 2010. Hydrogen evolution reaction. Handbook of fuel cells, 815.
Lefèvre, M., Proietti, E., Jaouen, F., Dodelet, J.P., 2009. Iron-based catalysts with improved oxygen reduction activity in polymer electrolyte fuel cells. Science 324 (5923), 71–74.
Li, J., Guan, Q., Wu, H., Liu, W., Lin, Y., Sun, Z., Lu, J., 2019b. Highly active and stable metal single-atom catalysts achieved by strong electronic metal–support interactions. J. Am. Chem. Soc. 141 (37), 14515–14519.
Li, X.F., Li, Q.K., Cheng, J., Liu, L., Yan, Q., Wu, Y., Luo, Y., 2016. Conversion of dinitrogen to ammonia by FeN3-embedded graphene. J. Am. Chem. Soc. 138 (28), 8706–8709.
Li, X., Zhao, Q., Feng, X., Pan, L., Wu, Z., Wu, X., Wu, M., 2019a. Pyridinic Nitrogen-Doped Graphene Nanoshells Boost the Catalytic Efficiency of Palladium Nanoparticles for the N-Allylation Reaction. ChemSusChem 12 (4), 858–865.
Liu, M., Wang, X., Liu, J., Wang, K., Jin, S., Tan, B., 2020. Palladium as a superior cocatalyst to platinum for hydrogen evolution using covalent triazine frameworks as a support. ACS Appl. Mater. Interfaces 12 (11), 12774–12782.
Mahmood, J., Li, F., Jung, S.M., Okyay, M.S., Ahmad, I., Kim, S.J., Baek, J.B., 2017. An efficient and pH-universal ruthenium-based catalyst for the hydrogen evolution reaction. Nat. Nanotechnol. 12 (5), 441–446.
Millet, P., Ngameni, R., Grigoriev, S.A., Mbemba, N., Brisset, F., Ranjbari, A., Etiévant, C., 2010. PEM water electrolyzers: From electrocatalysis to stack development. Int. J. Hydrogen Energy 35 (10), 5043–5052.
Monkhorst, H.J., Pack, J.D., 1976. Special points for Brillouin-zone integrations. Phys. Rev. B 13 (12), 5188.
Nie, R., Jiang, H., Lu, X., Zhou, D., Xia, Q., 2016. Highly active electron-deficient Pd clusters on N-doped active carbon for aromatic ring hydrogenation. Cat. Sci. Technol. 6 (6), 1913–1920.
Nørskov, J.K., Bligaard, T., Logadottir, A., Kitchin, J.R., Chen, J.G., Pandelov, S., Stimming, U., 2005. Trends in the exchange current for hydrogen evolution. J. Electrochem. Soc. 152 (3), J23.
Perry, M.L., Fuller, T.F., 2002. A historical perspective of fuel cell technology in the 20th century. J. Electrochem. Soc. 149 (7), S59.
Seh, Z.W., Kibsgaard, J., Dickens, C.F., Chorkendorff, I.B., Nørskov, J.K., Jaramillo, T.F., 2017. Combining theory and experiment in electrocatalysis: Insights into materials design. Science 355 (6321), eaad4998.
Singh, Y., Back, S., Jung, Y., 2018. Computational exploration of borophane-supported single transition metal atoms as potential oxygen reduction and evolution electrocatalysts. PCCP 20 (32), 21095–21104.
Steele, B.C., Heinzel, A., 2001. Materials for fuel-cell technologies. Nature 414 (6861), 345–352.
Sultan, S., Tiwari, J.N., Singh, A.N., Zhumagali, S., Ha, M., Myung, C.W., Kim, K.S., 2019. Single atoms and clusters based nanomaterials for hydrogen evolution, oxygen evolution reactions, and full water splitting. Adv. Energy Mater. 9 (22), 1900624.
Tiwari, J.N., Sultan, S., Myung, C.W., Yoon, T., Li, N., Ha, M., Kim, K.S., 2018. Multicomponent electrocatalyst with ultralow Pt loading and high hydrogen evolution activity. Nat. Energy 3 (9), 773–782.
Tripkovic, V., Vanin, M., Karamad, M., Björketun, M.E., Jacobsen, K.W., Thygesen, K. S., Rossmeisl, J., 2013. Electrochemical CO2 and CO reduction on metal-functionalized porphyrin-like graphene. J. Phys. Chem. C 117 (18), 9187–9195.
Vij, V., Sultan, S., Harzandi, A.M., Meena, A., Tiwari, J.N., Lee, W.G., Kim, K.S., 2017. Nickel-based electrocatalysts for energy-related applications: oxygen reduction, oxygen evolution, and hydrogen evolution reactions. ACS Catal. 7 (10), 7196–7225.
Vilé, G., Albani, D., Nachtegaal, M., Chen, Z., Dontsova, D., Antonietti, M., Pérez-Ramírez, J., 2015. A stable single-site palladium catalyst for hydrogenations. Angew. Chem. Int. Ed. 54 (38), 11265–11269.
Wang, Z.L., Choi, J., Xu, M., Hao, X., Zhang, H., Jiang, Z., Yamauchi, Y., 2020b. Optimizing Electron Densities of Ni-N-C Complexes by Hybrid Coordination for Efficient Electrocatalytic CO2 Reduction. ChemSusChem 13 (5), 929–937.
Wang, C., Gu, X.K., Yan, H., Lin, Y., Li, J., Liu, D., Lu, J., 2017. Water-mediated Mars–van Krevelen mechanism for CO oxidation on ceria-supported single-atom Pt1 catalyst. ACS Catal. 7 (1), 887–891.
Wang, B., Yue, Y., Jin, C., Lu, J., Wang, S., Yu, L., Li, X., 2020a. Hydrochlorination of acetylene on single-atom Pd/N-doped carbon catalysts: Importance of pyridinic-N synergism. Appl Catal B 272, 118944.
Wang, L., Zhu, C., Xu, M., Zhao, C., Gu, J., Cao, L., Lu, J., 2021. Boosting activity and stability of metal single-atom catalysts via regulation of coordination number and local composition. J. Am. Chem. Soc. 143 (45), 18854–18858.
Wu, G., More, K.L., Johnston, C.M., Zelenay, P., 2011. High-performance electrocatalysts for oxygen reduction derived from polyaniline, iron, and cobalt. Science 332 (6028), 443–447.
Xu, H., Cheng, D., Cao, D., Zeng, X.C., 2018. A universal principle for a rational design of single-atom electrocatalysts. Nat. Catal. 1 (5), 339–348.
Xu, W., Tang, H., Gu, H., Xi, H., Wu, P.F., Liang, B., Chen, W., 2022. Research progress of asymmetrically coordinated single-atom catalysts for electrocatalytic reactions. J. Mater. Chem. A.
Yuan, Y., Wang, J., Adimi, S., Shen, H., Thomas, T., Ma, R., Yang, M., 2020. Zirconium nitride catalysts surpass platinum for oxygen reduction. Nat. Mater. 19 (3), 282–286.
Zhang, B.W., Wang, Y.X., Chou, S.L., Liu, H.K., Dou, S.X., 2019. Fabrication of superior single-atom catalysts toward diverse electrochemical reactions. Small Methods 3 (9), 1800497.
Zheng, Y., Jiao, Y., Jaroniec, M., Qiao, S.Z., 2015. Advancing the electrochemistry of the hydrogen-evolution reaction through combining experiment and theory. Angew. Chem. Int. Ed. 54 (1), 52–65.